

## Supplementary materials

### Interfacial engineering of a multijunctional $\text{In}_2\text{O}_3/\text{WO}_3@\text{Ti}_4\text{N}_3\text{T}_x$ S-scheme photocatalyst with enhanced photoelectrochemical properties

Antony Okinyi Onjwaya<sup>a</sup>, Majahekupheleni Livileyise Malati<sup>a</sup>, Jane Catherine Ngila<sup>a</sup>,  
Langelihle Nsikayezwe Dlamini<sup>a,b\*</sup>

<sup>a</sup> University of Johannesburg, Doornfontein Campus, Department of Chemical Science, P.O. Box 17011, Doornfontein Campus, 2028, Johannesburg, South Africa.

<sup>b</sup> Centre for Nanomaterials Science Research, University of Johannesburg, South Africa.

\*Corresponding Author: [Indlamini@uj.ac.za](mailto:Indlamini@uj.ac.za)

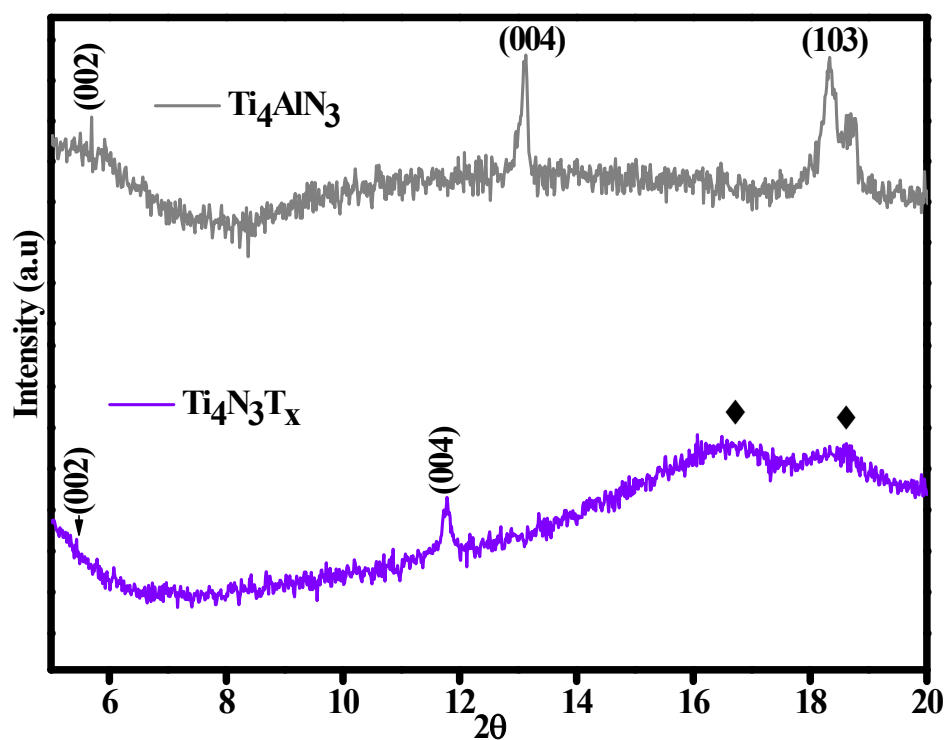
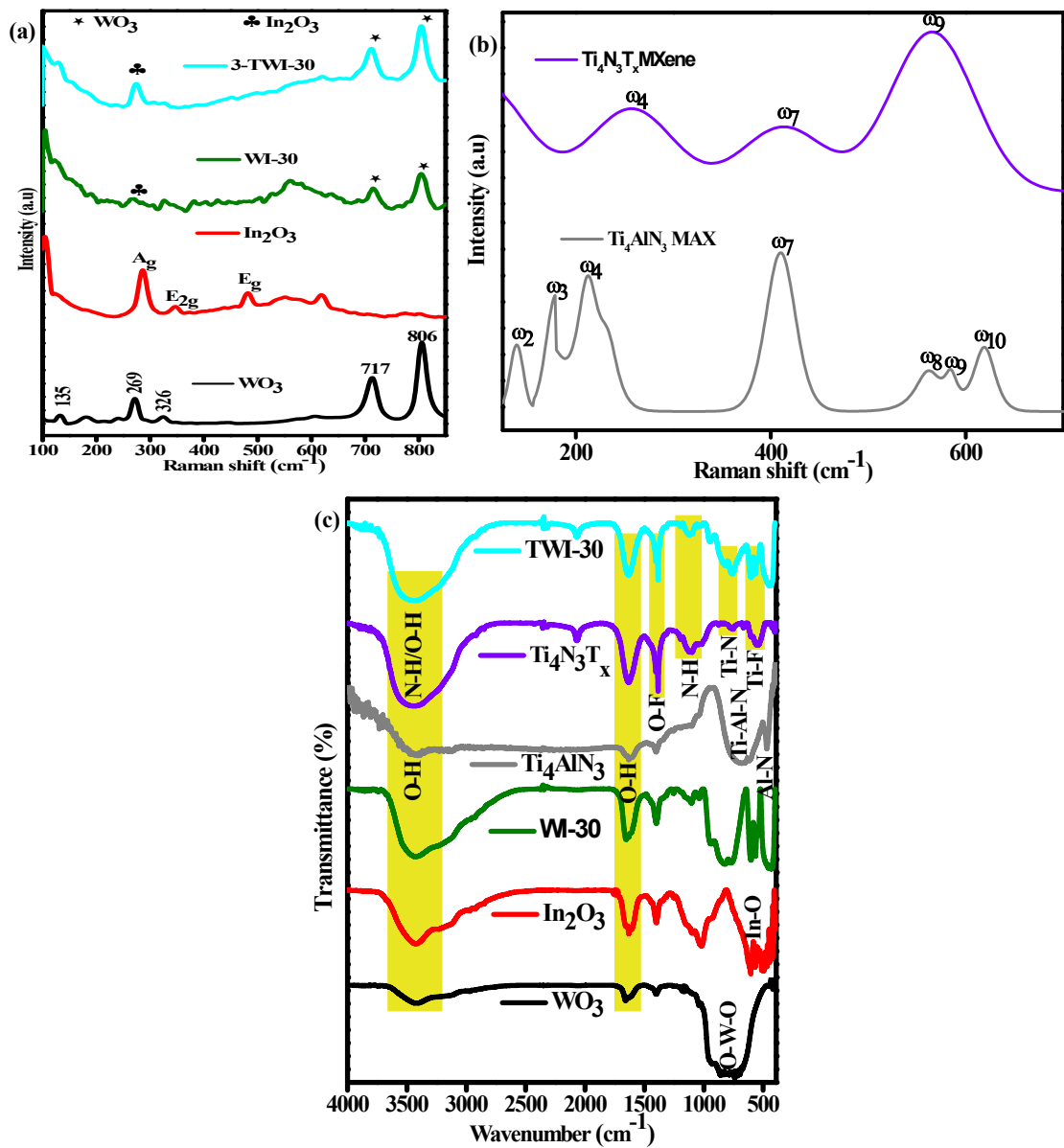
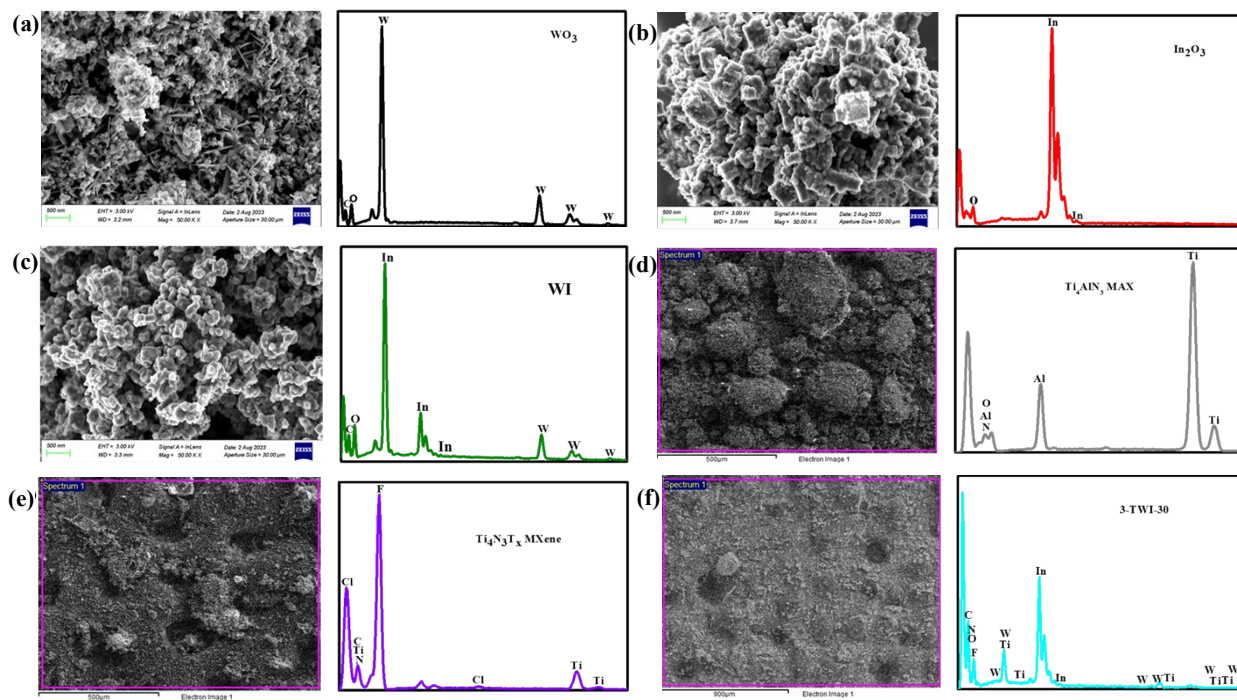


Figure S1: Deconvoluted XRD pattern for the  $\text{Ti}_4\text{AlN}_3$  MAX and  $\text{Ti}_4\text{N}_3\text{T}_x$  MXene.



**Figure S2:** (a, b) Raman spectra (c) FTIR spectrum for all synthesized materials.



**Figure S3.** SEM images for (a)  $WO_3$ , and (b)  $In_2O_3$ , (c)  $WO_3/In_2O_3$  binary nanocomposites, (d) MAX, (e) MXene, (f) ternary nanocomposites.

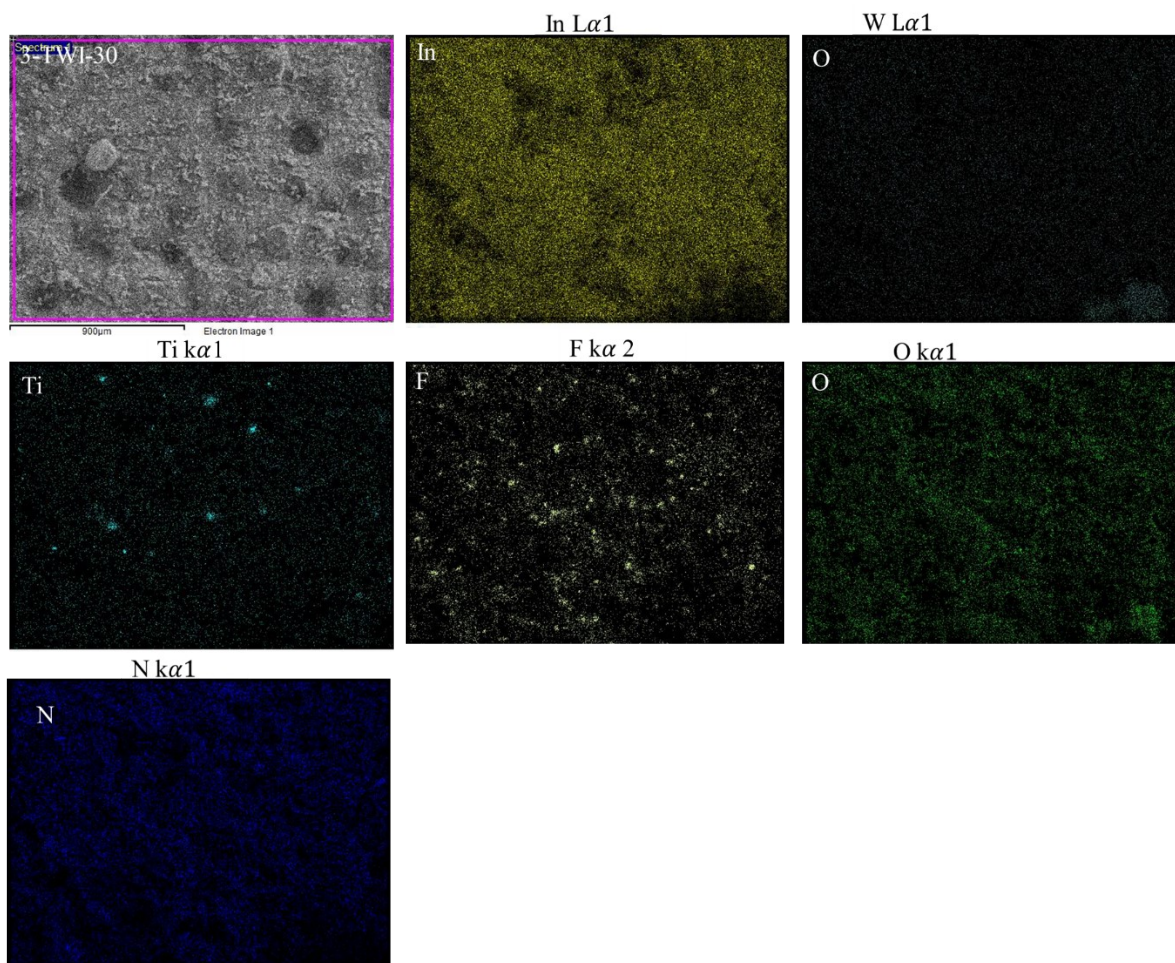


**Figure S4:** Elemental mapping for the ternary 3-TWI-30 composite.

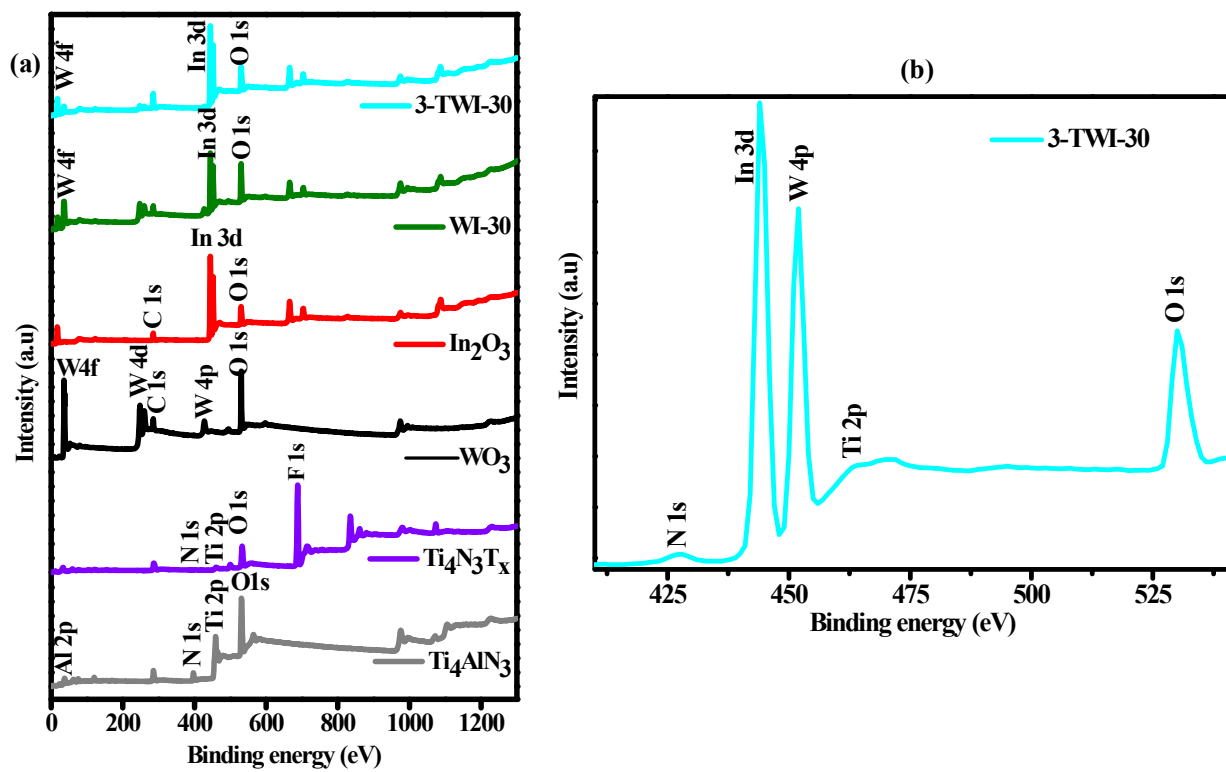


**Figure S5:** (a) XPS survey scan spectra spectrum of the as-prepared materials, (b) magnified 3-TWI-30 survey.

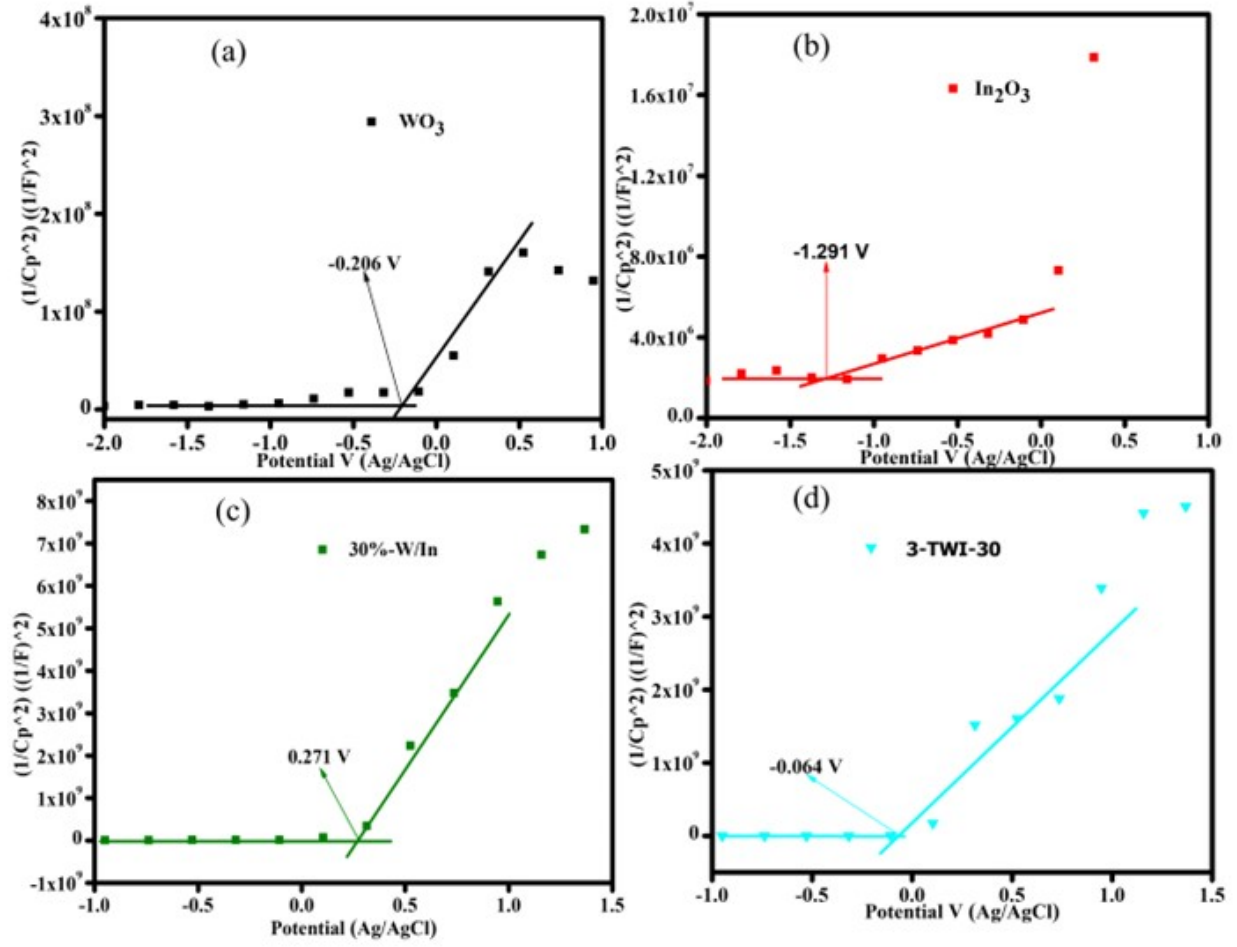


**Figure S6:** Mott–Schottky (MS) curves for (a)  $\text{WO}_3$ , (b)  $\text{In}_2\text{O}_3$ , (c) binary nanocomposites and (d) ternary nanocomposite.

**Table S1:** Flat band potential ( $V_{\text{FB}}$ ), valence band potential ( $E_{\text{VB}}$ ), conduction band potential ( $E_{\text{CB}}$ ), Mott–Schottky plot slope ( $\text{MS}_{\text{slope}}$ ) and charge-carrier concentration ( $N_{\text{D}}$ ).

Sample	$V_{\text{FB}}$ (V vs Ag/AgCl)	$E_{\text{CB}}$ (V vs. NHE)	$E_{\text{VB}}$ (V vs. NHE)	$\text{MS}_{\text{slope}}$ ( $\text{cm}^2/\text{C.F}) \times 10^9$	$N_{\text{D}}$ ( $\text{cm}^{-3}) \times 10^{21}$
$\text{WO}_3$	-0.206	-0.246	+1.88	2.45	11.05
$\text{In}_2\text{O}_3$	-1.291	-1.204	+1.41	2.54	6.25
WI-30	+0.271	+0.206	+2.28	7.52	2.70
3-TWI-30	-0.064	+0.060	+2.34	2.59	7.83

Effective photocatalytic performance largely depends on the photocatalyst's surface area and porosity.<sup>1</sup> Photocatalytic active sites are generally exposed due to the rich porous structures of the photocatalyst.<sup>2</sup> The pore structure, pore volume and surface area of WO<sub>3</sub>, In<sub>2</sub>O<sub>3</sub>, WI-30 and 3-TWI-30 fabricated photocatalysts were studied using nitrogen adsorption-desorption isotherms. The obtained Brunauer-Emmett-Teller (BET) specific surface area, pore volume, and pore size are summarized in **Table S2**. All the as-synthesized materials show a type IV isotherm shape and type H2 hysteresis corresponding to a mesoporous structure (pore size 2 to 50 nm) as indicated in **Figure S7a insert, b**.<sup>3-5</sup> The Burrett-Joyner-Holenda (BJH) for the pristine WO<sub>3</sub> and In<sub>2</sub>O<sub>3</sub> were 48.06 and 30.207 nm respectively (**Figure S7c**). Upon the fabrication of the binary composite, the pore size decreased to 27.253 nm (**Figure S7c**). Binary formation leads to the coverage of the individual pores, thus reducing their distributions.

Ti<sub>4</sub>AlN<sub>3</sub> MAX recorded a pore size of 23.458 nm. Upon etching Al layer, there was observed increase in the pore size to 29.969 nm in Ti<sub>4</sub>N<sub>3</sub>T<sub>x</sub> (**Figure S7d**). Removal of the Al layer resulted into increased pore distribution. The ternary composite recorded an increment in pore size of 27.764 nm compared to binary composite (**Figure S7d**). This is attributed to the added porous MXene. However, the ternary composite showed a lower pore size compared to the pristine materials. During the crystal growth, the binary crystals are sandwiched in the MXene layer resulting into the coverage of the porous sites.

The BET surface areas for pure WO<sub>3</sub> and In<sub>2</sub>O<sub>3</sub> were 15.410 and 5.527 m<sup>2</sup>/g, respectively. Upon the formation of the WI-30 binary and 3-TWI-30 ternary composites, the BET surface area substantially increased to 22.383 m<sup>2</sup>/g in 3-TWI-30 ternary composite. Loading of Ti<sub>4</sub>N<sub>3</sub>T<sub>x</sub> onto WI-30 binary composite increased the specific surface area of the ternary composite. This exposes an increased surface area in the layered ternary heterostructure for irradiation by incident light and thus more active photocatalytic sites can be obtained, thus enhancing the photocatalytic performance.<sup>6</sup> It is worth noting that high BET surface area, pore size, and pore volume are highly desirable as they are beneficial in improving the photocatalytic degradation activity of a photocatalyst. Thus, more pollutants can be adsorbed on the designed heterostructure photocatalyst's high surface area.<sup>7</sup>

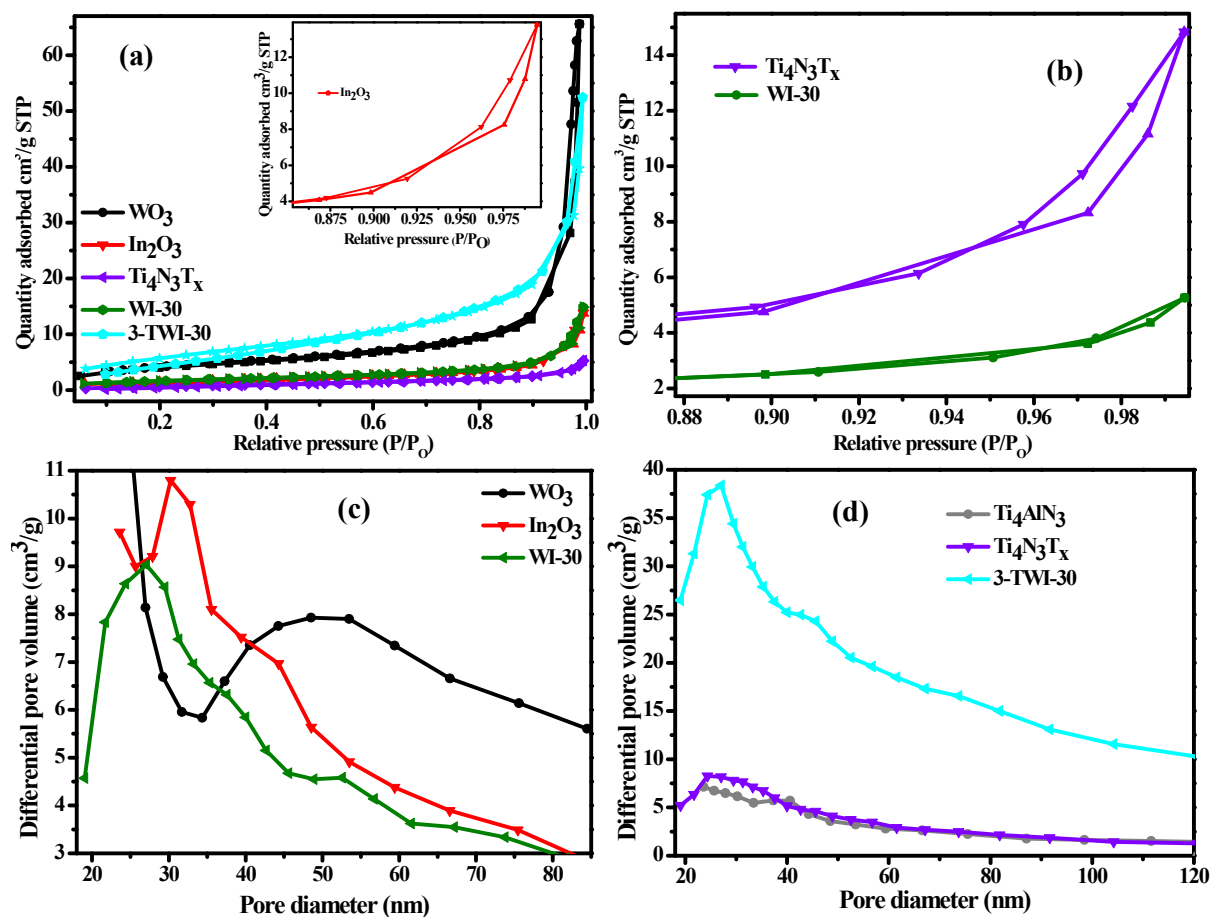


**Figure S7:** (a) N<sub>2</sub> adsorption-desorption isotherms of the as-synthesized materials, (b, c) deconvoluted isotherms and (d, e) pore size distribution for pristines and nanocomposite.

**Table S2:** BET surface area, pore volume and pore size for the as-synthesized nanomaterials.

Photocatalyst	BET surface area (m <sup>2</sup> /g)	Pore Volume (cm <sup>3</sup> /g)	Pore Size (nm)
WO <sub>3</sub>	15.410	0.101	48.060
In <sub>2</sub> O <sub>3</sub>	5.527	0.021	30.207
Ti <sub>4</sub> AlN <sub>3</sub>	2.731	0.012	23.458
Ti <sub>4</sub> N <sub>3</sub> T <sub>x</sub>	3.054	0.008	29.969
WI-30	6.103	0.022	27.253
3-TWI-30	22.38	0.081	27.764

## Notes and References

1. Gao K, Hou L-a, An X, Huang D, Yang Y. BiOBr/MXene/gC<sub>3</sub>N<sub>4</sub> Z-scheme heterostructure photocatalysts mediated by oxygen vacancies and MXene quantum dots for tetracycline degradation: Process, mechanism and toxicity analysis. *Applied Catalysis B: Environmental*. 2023/04/01/ 2023;323:122150. doi:<https://doi.org/10.1016/j.apcatb.2022.122150>
2. Tu W, Liu Y, Chen M, et al. Carbon nitride coupled with Ti<sub>3</sub>C<sub>2</sub>-Mxene derived amorphous Ti-peroxo heterojunction for photocatalytic degradation of rhodamine B and tetracycline. *Colloids and Surfaces A: Physicochemical and Engineering Aspects*. 2022/05/05/ 2022;640:128448. doi:<https://doi.org/10.1016/j.colsurfa.2022.128448>
3. Bardestani R, Patience GS, Kaliaguine S. Experimental methods in chemical engineering: specific surface area and pore size distribution measurements—BET, BJH, and DFT. *The Canadian Journal of Chemical Engineering*. 2019;97(11):2781-2791.
4. Wu Y, Li X, Yang Q, et al. Mxene-modulated dual-heterojunction generation on a metal-organic framework (MOF) via surface constitution reconstruction for enhanced photocatalytic activity. *Chemical Engineering Journal*. 2020/06/15/ 2020;390:124519. doi:<https://doi.org/10.1016/j.cej.2020.124519>
5. Ramachandran R, Rajavel K, Xuan W, Lin D, Wang F. Influence of Ti<sub>3</sub>C<sub>2</sub>T<sub>x</sub> (MXene) intercalation pseudocapacitance on electrochemical performance of Co-MOF binder-free electrode. *Ceramics International*. 2018/08/15/ 2018;44(12):14425-14431. doi:<https://doi.org/10.1016/j.ceramint.2018.05.055>
6. Wang H, Wu Y, Xiao T, et al. Formation of quasi-core-shell In<sub>2</sub>S<sub>3</sub>/anatase TiO<sub>2</sub>@metallic Ti<sub>3</sub>C<sub>2</sub>T<sub>x</sub> hybrids with favorable charge transfer channels for excellent visible-light-photocatalytic performance. *Applied Catalysis B: Environmental*. 2018;233:213-225.
7. Zhang M, Duo F, Lan J, et al. In situ synthesis of a Bi(2)O(3) quantum dot decorated BiOCl heterojunction with superior photocatalytic capability for organic dye and antibiotic removal. *RSC Adv*. Feb 14 2023;13(9):5674-5686. doi:10.1039/d2ra07726d